https://doi.org/10.1016/j.conbuildmat.2020.121305

The following publication Yang, S., Jiang, J., Leng, Z., & Ni, F. (2021). Feasibility and performance of the Semi-circular Bending test in evaluating the low-temperature performance of asphalt mortar. Construction and Building Materials, 269, 121305 is available at https://doi.org/10.1016/j.conbuildmat.2020.121305.

Feasibility and Performance of the Semi-circular Bending Test in Evaluating the Low-temperature Performance of Asphalt Mortar

Abstract: Semi-circular Bending (SCB) test has been widely used to evaluate the fracture performance of asphalt mixtures, but its potential in evaluating the low-temperature performance of asphalt mixtures at mortar scale has been seldom investigated. This study aims to explore the feasibility and evaluate the performance of SCB tests in evaluating the low-temperature performance of asphalt mortar. To quantify the influence of the crushing and local creep at the top of the SCB test samples on testing results, the Digital Image Correlation (DIC) method was used to characterize the displacement field of mortar samples during the test under different loading rates at -10°C. The effects of binder film thickness, filler content, and aging condition on low-temperature performance of asphalt mortar were investigated by SCB test. The experimental design set a fixed nominal maximum aggregate size of 4.75mm. The test matrix considered three binder film thicknesses (9, 10 and 11μm) and four filler contents (8.5%, 9.4%, 10.5% and 11%) at two aging conditions (short-term and long-term aging). Two cracking indexes including before-peak slope (S_{bp}) and fracture energy (G_f) were used to evaluate the low-temperature performance. According to the results of DIC analysis, the loading rate of 3mm/min was proposed to be the optimum for the SCB mortar test at -10°C. It was concluded that the SCB mortar test can effectively differentiate the low-temperature cracking performance of different asphalt mortars under different aging conditions. Thicker binder film thickness can significantly decrease the aging rate of asphalt mortar from short-term aging to long-term aging, whereas the effect of filler content on ageing rate is not statistically significant.

Keywords: Asphalt mortar, Low-temperature cracking, SCB test, Digital image correlation, Aging.

1. Introduction

Asphalt mixtures can be analyzed in four different scales, including asphalt binder, mastic (binder and filler), mortar or Fine Aggregate Matrix (FAM) and asphalt mixtures [1][2]. Low-temperature cracking is one of the major distresses of asphalt pavement [3][4]. Based on the observation of the separated surface of the mineral aggregate within the asphalt mixtures at low temperature, the failure modes of the low-temperature cracking can fall into two categories: adhesion failure and cohesion failure [5]. The former refers to the separation between binder and mineral aggregate [6], while the latter refers to the separation within the asphalt binder itself [7]. Recent research has shown that the cohesive strength of asphalt mortars at low temperature can significantly affect the cracking resistance of asphalt pavement [8][9], because the fatigue cracks and thermal cracks propagate within mortar or FAM of asphalt mixtures [10][11].

Compared with the fracture tests for asphalt mixture samples [12][13], the tests for asphalt mortar samples have some advantages, such as material saving, lower test variability, and easier sample preparation [14]. The mix design of mortar varies in terms of Nominal Maximum Aggregate Size （NMAS）, asphalt content and air void distribution based on different hypotheses. Also, the mechanical properties of the asphalt mortar are extremely sensitive to the volumetric changes [15]. However, when mortar is evaluated for comparison, it is not necessary to replicate them exactly same as that in the mixtures if the samples are fabricated following the same procedure [16]. Currently, most of the performance tests for asphalt mortar are performed by using Dynamic Shear Rheometer (DSR) or Bending Beam Rheometer (BBR). The mainly evaluated properties of mortar include viscoelastic properties through DSR strain/stress sweep tests [17], fatigue and healing characteristics through DSR time sweep and creep and recovery tests [18][19], and fracture/moisture damage resistance at low temperature through BBR tests [20]. The BBR test is usually used to capture the creep stiffness (S) and rate of relaxation (m-value) of the mortar samples in beam geometry [21][22]. Besides, to simulate the fracture process of the asphalt mortar at

low temperature, the Single Edge Notched Bending (SENB) test has been developed by adding a notch on the BBR sample [23]. However, the fabrication of the beam samples by static compression in steel mold is complicated. In addition, when the NMAS of mortar is larger than 2.36mm, the fine aggregate particles become larger than half the size of the bending beam sample.

The above studies demonstrated that asphalt mortar plays a key role in the cracking resistance of asphalt mixtures. Thus, it can be valuable to the evaluation of the cracking resistance of asphalt mixtures. However, no quantitate model has been established between the mesoscopic indexes (or volumetric indexes of mortar) and the cohesive parameters of asphalt mortar at low temperature. Besides, the relationship between the mix design of mortar and the low-temperature cracking performance has not been clearly understood yet. Therefore, to extend the application range of the mortar testing and simplify the fabrication of the mortar samples, the SCB test configuration in a Universal Testing Machine (UTM) is proposed in this study to investigate the low-temperature performance of asphalt mortar [24]. The SCB samples were initially used to test mode I fracture toughness of rock and other brittle materials [25]. Afterwards, it has been widely used and improved to investigate the fracture flexibility and fatigue cracking of asphalt mixtures under monotonic or cyclic loading [26][27]. The effects of factors from both the external test conditions and material properties on the low-temperature cracking performance of asphalt mixtures have been extensively studied [28]. It was found that the fracture characteristic of asphalt mixtures is rate and temperature dependent in SCB test [29]. Also, the variation of fracture energy measured by SCB test at low temperature can be significantly affected by air void, type of aggregate and type of binder modifier [30]. In addition, the oxidation aging can influence the low-temperature cracking performance of asphalt mixtures significantly [31]. The more the pavement aged, the greater the incidence that thermal cracking would occur. Therefore, like the research of asphalt mixture samples, it is reasonable to investigate the factors that can significantly affect the low-temperature cracking of asphalt mortar samples from both

the external test conditions and the material properties. Because asphalt mortar uses smaller NMAS, while remains the sample size level as asphalt mixture sample, asphalt mortar SCB sample is easy to meet the requirement of Representative Volume Element (RVE) size. Thus, it is expected that SCB test with asphalt mortar samples may capture the fracture energy with higher consistency.

2. Objectives

The main objectives of the study include:

- to validate the load-displacement curves from the SCB test at the mortar scale based on the DIC methods considering the variation of loading rates;
- to analyze the difference of the fracture energy and bending stiffness of the asphalt mortars with different combinations of binder film thickness, and filler content; and
- to investigate the influence of both binder film thickness and filler content on the aging rate of the asphalt mortar.

3. Materials and Mortar Design

A styrene–butadiene–styrene (SBS) polymer-modified asphalt binder (PG76-22) and the limestone filler (passing the 0.075mm size sieve) combined with fine granite aggregate (passing the 4.75mm size sieve) were used in this study to fabricate the asphalt mortar samples. As Figure 1 shows, the standard gradation of the mortar is converted from a common dense-graded gradation with a NMAS of 13mm. The filler content of the standard mortar gradation is 9.4% by weight of all mineral aggregate. Another three filler contents of 8.5%, 10.5% and 11% were also applied on the fixed gradation curve from 4.75mm to 0.075mm to evaluate the influence of filler contents on the cracking performance of asphalt mortar. At the same time, three different binder film thicknesses including 9, 10 and 11μm were selected to investigate the effect of binder content on the cracking of mortar. As defined in Equation 1 and 2, the specific surface areas (SA) and the effective binder content (P_{be}) of each combination of the mortar with different filler contents and binder film thicknesses were calculated

according to the Chinese specification of JTG F40-2004, "Technical Specifications for Construction of Highway Asphalt Pavements". The detailed volumetric properties of different mortars are listed in Table 1. Two aging conditions were considered: Short Term Oven Aging (STOA) according to AASHTO R30 recommendation with four hours loose mixture aging at 135ºC, and Long-Term Oven Aging (LTOA) according to the procedure of 12 hours loose mixture aging at 135ºC.

$$SA = 10 \times (0.41 + 0.0041P_{4.75} + 0.0082P_{2.36} + 0.0164P_{1.18} + 0.02877P_{0.6} + 0.0614P_{0.3} + 0.122P_{0.15} + 0.3277P_{0.075}) \quad (1)$$

$$T = \frac{P_{be}}{\gamma_b \times SA} \quad (2)$$

where SA= the specific surface area, cm^2/g; P_i = the corresponding passing percentage of sieve size i, %; P_{be} = the effective binder content, %; T = the binder film thickness, μm; and γ_b = the specific density of the binder.

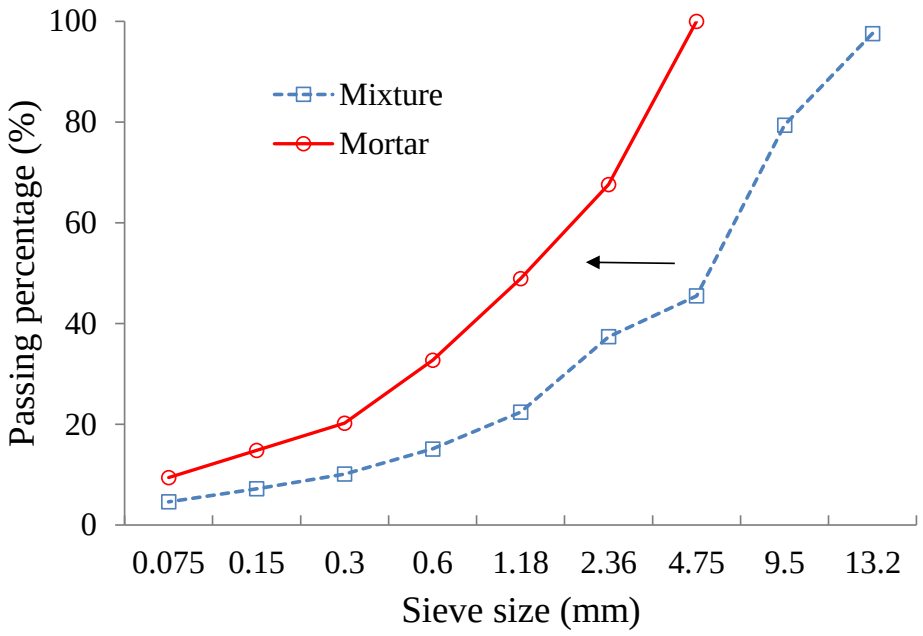

Figure 1 Gradation curves of the asphalt mixtures and the corresponding mortar.

Table 1 Volumetric properties of the asphalt mortar.

Mortar ID	Binder film thickness, T (μm)	Filler content (%)	Specific surface area, SA (cm^2/g)	Effective Binder content, P_{be} (%)
F 8.5-T 9*	9	8.5	87.5	7.8
F 8.5-T 10	10	8.5	87.5	8.9
F 8.5-T 11	11	8.5	87.5	9.6
F 9.4-T 9	9	9.4	92.4	8.3
F 9.4-T 10	10	9.4	92.4	9.4
F 9.4-T 11	11	9.4	92.4	10.2
F 10.5-T 9	9	10.5	98.0	8.8
F 10.5-T 10	10	10.5	98.0	10.0
F 10.5-T 11	11	10.5	98.0	10.8
F 11-T 9	9	11.0	100.8	9.1
F 11-T 10	10	11.0	100.8	10.2
F 11-T 11	11	11.0	100.8	11.1

* F 8.5-T 9 means asphalt mortar with a filler content of 8.5% and binder film thickness of 9μm.

4. Test Methods

4.1 SCB test for mortar

A Universal Testing Machine (UTM) equipped with 25kN load cell and an environment chamber was used to perform the SCB mortar test. The setup for the SCB mortar test consists of a loading ramp at the top center of the sample, and two supporting rollers at two sides of the bottom, with a distance of 80mm, which is 0.8 times of the diameter of the mortar sample. During the SCB mortar test, a constant pre-defined displacement rate was applied to the sample until the cracking failure occurs. There were seven loading rates including 0.75, 1, 3, 15, 30, 50 and 80mm/min. The low testing temperature was set at -10°C. According to AASHTO TP105, the SCB test with PG76-22 binder needs to be performed at -24°C and -12°C. However, there are three reasons that this study chose to perform the SCB test at -10°C. First, it is exceedingly difficult for normal equipment to reach the low temperature as -24°C. The equipment used in this study cannot provide such low temperature in the environmental chamber. Second, this research studied the local material to support the

local pavement construction in southern part of China, -10°C is the normally used temperature here to evaluate the low temperature performance of asphalt. Third, this research did not intend to study the influence of test temperature on SCB fracture test, but it would be interested to test asphalt mortar at lower temperature with upgraded equipment. In addition, since the inhomogeneous composite of the asphalt mortar consisting of aggregate particles with different sizes and binders with different thickness distribution, the size effect on the testing results might be amplified when the testing samples scale are small [32][33]. This study did not perform a RVE (Representative Volume Element) analysis regarding to the sample size effect. However, since gradation of asphalt mortar is fine, this study use 100mm diameter samples to control the variation of the test results. And smaller sample size can help with the sample frication. The thickness of the SCB sample was set at 33mm. No notch was applied to the samples. The notch configuration options for SCB test include but not limited to regular saw cut rectangular notch, pre-fatigue notch, semi-circular notch. Also, Non-notch is also an option. There are both advantages and disadvantages for each of the option. Pre-fatigue notch is perfect in fracture theory because it provides a sharp notch tip, however, it is not very practical in asphalt specimen mainly because it is easy to damage the specimen during the pre-fatigue process. A normal saw cut rectangular notch cannot provide a sharp notch tip, but it is relatively practical. While semi-circular notch configuration does not have a sharp tip to isolate the crack initiation, but it can control the notch initiation in the “semi-notch” area. Finally, non-notched sample does not provide notch tip at all. The disadvantage of non-notch is that the crack initiation cannot be controlled to occur at certain area. But the stress in non-notch sample can concentrate at the weakest defect to initiate a crack. The non-notched fracture test may represent how crack initiates in the field most closely, but this assumption needs to be proved by research. This research did not study the influence of the notch configuration and choose to use the non-notched SCB test for its advantages. All samples tested in this study were produced by the Superpave Gyratory Compactor (SGC) with a target air void content of 4±0.5%. As illustrated in Figure 2(a), the cylindrical samples with a diameter of 100mm and a

height of 100mm were fabricated first. Then two mortar circles with a target thickness of 33mm were cut from the middle of the original sample by a masonry saw. After that, the circle was cut into two halves along the diameter. The volumetric properties of each half were tested, and the air void content of the samples was controlled within the range from 3.5% to 4.5%. The load-displacement relation was captured by a vertically Linear Variable Differential Transformer (LVDT) mounted on the top of the sample. Three replicates were prepared for each SCB mortar test.

4.2 Incorporation of the DIC system

The DIC method was used to obtain the full-field displacements and strains of the front surface of the sample by taking continuous images of the surface by a high-speed industry camera, which collects 8-bit grey scale images with 18-megapixel resolution. The frame rate of the camera was set at 14 fps. Before the implementation of the DIC instrument, a series of surface treatments on sample surface was applied. First, as shown in Figure 2 (b) and (c), the surface of the samples were painted uniformly matt white coupled with random black dots on it, which can provide a random and uniform speckle pattern on the front surface of the sample. Thus, the displacement/strain of each black dot during the loading can be captured based on the measurement and analysis of the continuous images. A camera was placed carefully to make sure the captured images of the sample are clear. The frame rate was set at 5 fps in the SCB mortar test. Two white lights were mounted on both sides of the sample to improve the illumination. A post image analysis was conducted to capture the displacements/strain field on the sample surface. The Gauss-Newton algorithm [34] was used as a sub-pixel registration algorithm in the displacement measurement. A numerical differentiation process was used to obtain the strain considering the noise contained in the computed displacement [35].

In this study, the DIC method was mainly applied to verify the vertical deformation of the mortar sample during the SCB test, due to the fact that significant local deformation can be observed near the loading strip on the top of the sample as shown

in Figure 2(d). As seen in Figure 2(e), the vertical displacements of the five points located on the sample surface (start from the top edge on the center axis of the sample with an interval of 1cm,designated as point 1, point 2, point 3, point 4 and point 5), were measured in the test. The displacement of each point and the relative displacement between any two points can be captured.

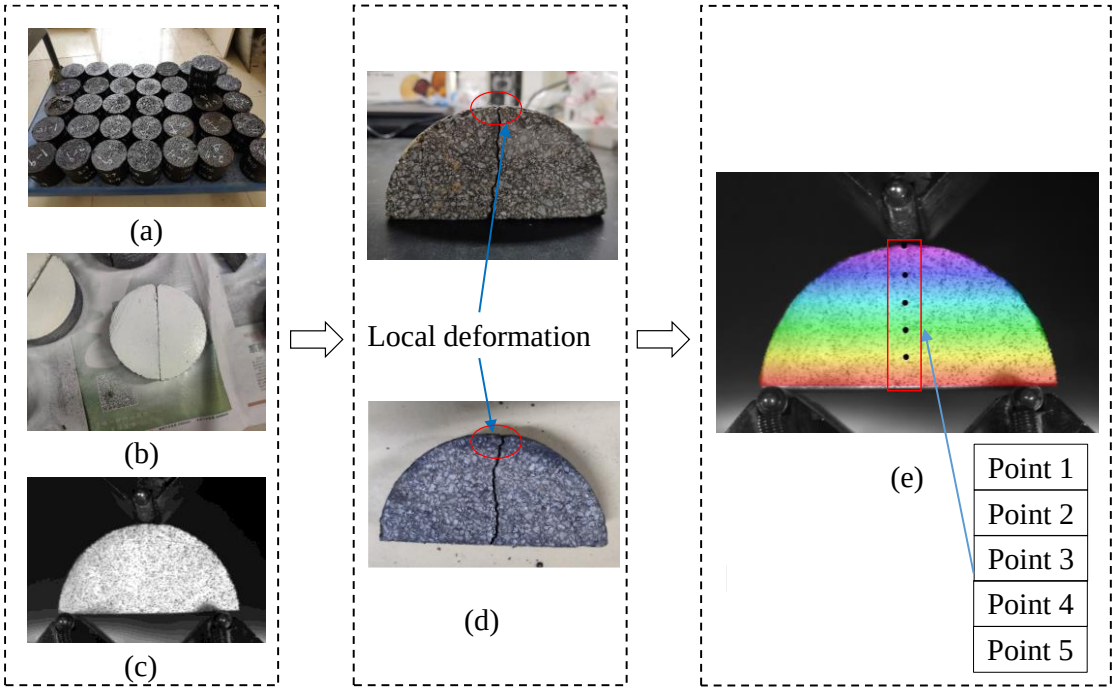

Figure 2 Setup of the SCB mortar test with DIC system: (a) SGC samples; (b) surface treatment; (c) speckle pattern of the front surface; (d) the cracked sample; and (e) measurement point locations.

4.3 Definition of the cracking indexes

Figure 3 demonstrates a typical load-displacement curve of the SCB motor test performed at a low temperature. With a certain vertical displacement rate, the vertical load increases with increasing growth rate, and then decreases sharply. A polynomial equation with a degree of three shown in Equation 3 was used to fit the before-peak curve of the SCB mortar test. Two independent indexes were defined to characterize the load-displacement curve including the before-peak slope (S_{bp}) and the fracture energy (G_f). In terms of the before peak slope (S_{bp}), it was defined as the slope of the load-displacement curve at the inflection point before the peak load. AASHTO TP124

defines the post-peak slope as one input for the flexibility index, or FI. This study used the before-peak slope instead of the specification defined post-peak slope for the following three reasons. First, this study intended to reduce the creep damage at SCB sample top, thus, the loading rate selected in this study was relatively high. Therefore, most of the fracture tests were quite brittle and the load-displacement curve were not softening curve, and the post-peak slope is infinite. Second, the before-peak slope represents the stiffness of the material that can characterize the crack initiation of the material. Compare to the crack propagation, the initiation is relatively more important because once the crack initiates, the crack usually propagates fast and the pavement must be treated. Third, flexibility index is normally measured at intermediate temperature but tests in this study were run at low temperature.

The fracture energy (G_f) calculation is shown in Equation 4. Higher S_{bp} indicates stiffer or more brittle mortar, and higher G_f indicates that the mortar needs to consume more energy to form a crack [36].

$$F_{bp}(u) = c_1 \times u^3 + c_2 \times u^2 + c_3 \times u + c_4 \tag{3}$$

$$G_f = \frac{W_f}{H \cdot T} \tag{4}$$

where F_{bp} = load of before-peak stage, kN; u = vertical displacement, mm; c_1, c_2, c_3, c_4 = fit coefficient of the polynomial equation; G_f = fracture energy, J/m^2; W_f = the total area within the load-displacement curve, J; H = sample height, m; and T = sample thickness, m.

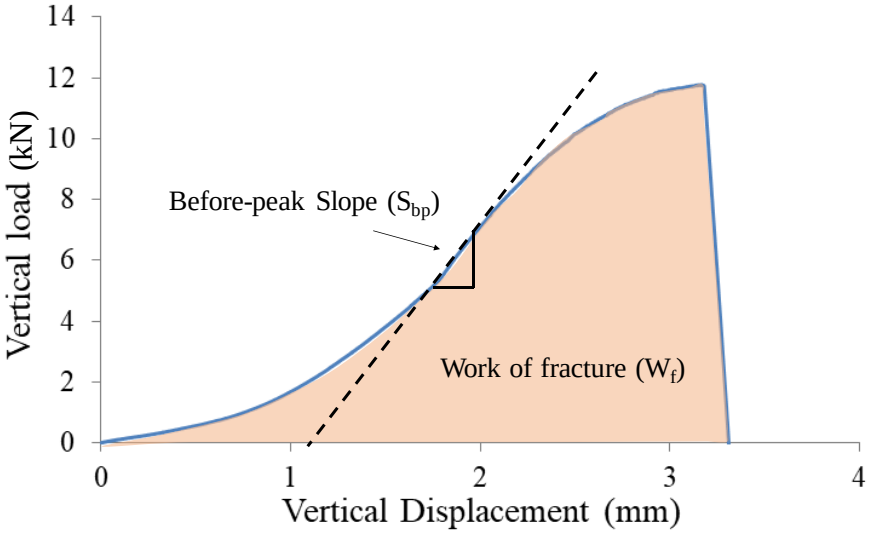

Figure 3 Definition of the fracture indexes based on the SCB mortar test.

5. Discussion of Test Results

5.1 Analysis of the vertical deformation in SCB test

5.1.1 Quantification of the creep curves

Based on the DIC system, the full-displacement, and strain on the front surface of samples can be captured. The plots of displacement versus image (or time) number of certain locations illustrated in Figure 2(e) could be obtained. The corresponding displacement versus time/image number of the loading roller was recorded by the vertically LVDT mounted on the top of the edge simultaneously. Figure 4 demonstrates the vertical deformation of the pre-defined five points calculated by the DIC system and the corresponding vertical deformation captured by the LVDT. It was found that the vertical displacement measured by LVDT and the calculated deformation of DIC (point 1) overlapped with each other, which indicates that this DIC system can achieve acceptable accuracy in deformation measurement. The deformation measured by point 1 was significantly different from the deformation measured by other points. The deformation curves of point2, point 3, point 4 and point 5 almost overlapped with each other. Thus, this result indicates that most of the compressive creep deformation occurs within the local region between point 1 and point 2, which is the top 1cm area next to the top roller in the vertical direction. It

could also be observed that the relative difference between deformation curves of point 1 (or LVDT) and point 2 was negligible when the vertical deformation was low (less than 1mm in Figure 4), but the difference accumulated fast when the vertical deformation increased.

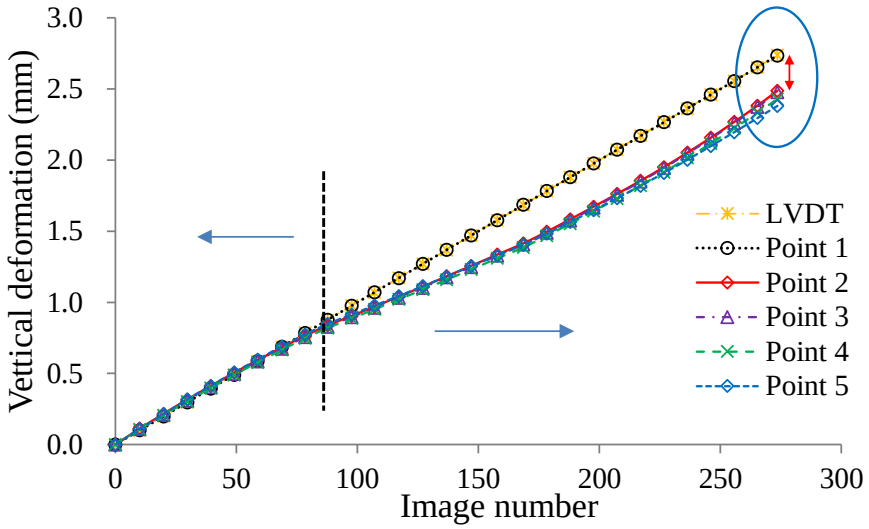

Figure 4 Vertical deformation of a mortar sample at the loading rate 3mm/min.

Figure 5(a) illustrates the visualized local deformation of the mortar sample after the monotonic loading with different loading rates. Three typical loading rates, including 0.075, 3 and 30mm/min, were selected for the comparison. At each loading rate, the images before loading and before cracking were used to analyze the local deformation caused by the monotonic load from the upper roller. It could be found that crushing occurred under the narrow loading strip when the loading rate was 0.075mm/min, while no obvious crushing occurred at the loading rate of 3 and 30mm/min. In addition, local deformation could still be observed under the loading strip when loading rate was 3mm/min, whereas no obvious deformation occurred under the loading rate of 30mm/min. To quantify the local deformation of the mortar samples under varying loading rates, the creep curves were calculated by subtracting the load-displacement curves measured from LVDT and point 2. As Figure 5(b) shows, the local deformation of mortar samples at the loading rate of 0.075mm/min was approximately 1.5mm, while only approximately 0.3mm at the loading rate of

3mm/min, and approximately 0.1mm at the loading rate of 30mm/min.

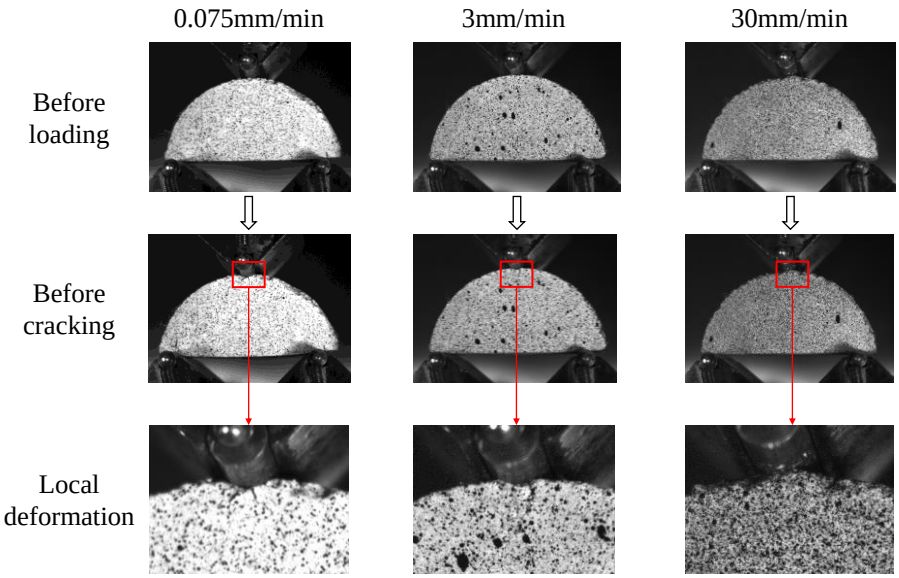

(a)

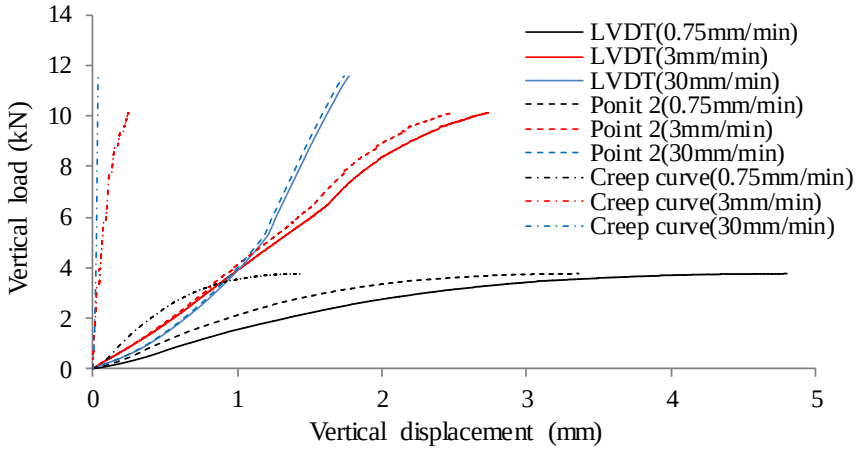

(b)

Figure 5 Observation and quantification of the local deformation during the monotonic loading: (a) images recorded by the camera; (b) creep curves.

5.1.2 Influence of the vertical creep on the cracking indexes

As shown in Figure 5(b), both the load-displacement curves obtained from LVDT data and DIC data can be used to calculate the cracking indexes, including before-peak slope (S_{bp}) and fracture energy (G_f). By comparing the cracking indexes from both load-displacement curves, the influence of the vertical creep on the results of the cracking indexes could be evaluated. Figure 6 exhibits the cracking indexes of both S_{bp} and G_f and the relative errors of the indexes from both load-displacement curves at

different loading rates from 0.075 to 80mm/min. Since asphalt binder is a viscous-elastic material followed the time-temperature principle [37], similar to the SCB test conducted on asphalt mixtures, it is reasonable to assume that loading time or temperature can also significantly influence the testing results of asphalt mortar. In Figure 6(a), as the loading rate increases, the S_{bp} of the mortar samples from load-displacement curves by both LVDT data and DIC data increase. However, the S_{bp} calculated by DIC data (point 2) is always higher than the S_{bp} calculated by LVDT data due to the extraction of the local creep deformation. The relative error of S_{bp} between two data sets from point 2 and LVDT decreases sharply when the loading rate increases from 0.075mm/min to 3mm/min. Then, the error remains at the low level when the loading rate is higher than 3mm/min. As can be seen in Figure 6(b), with the increment of the loading rate, the G_f firstly increases then decreases. G_f reaches its peak value when the loading rate is 3mm/min. The G_f calculated by load-displacement curves from point 2 is always lower than that from the LVDT due to the extraction of the dissipated energy caused by creep deformation. The relative error of G_f between two data sets from point 2 and LVDT decreases sharply when the loading rate increases. Besides, the coefficient variation (COV) of the relative errors of both S_{bp} and G_f are lower than 5% when the loading rate is higher than 3mm/min. The results of S_{bp} and G_f show higher variance when the loading rate is 0.075 or 1 mm/min. Considering both the relative error and variation of the error, the loading rate of 3mm/min is finally recommended to be one acceptable loading rate for the mortar SCB test at testing temperature of -10ºC. Since the relative errors of both the S_{bp} and G_f caused by the local deformation are less than 10%, and the variation of the relative errors caused by the local compressive creep are less than 5%, the error caused by the local deformation is considered as steady and predictable.

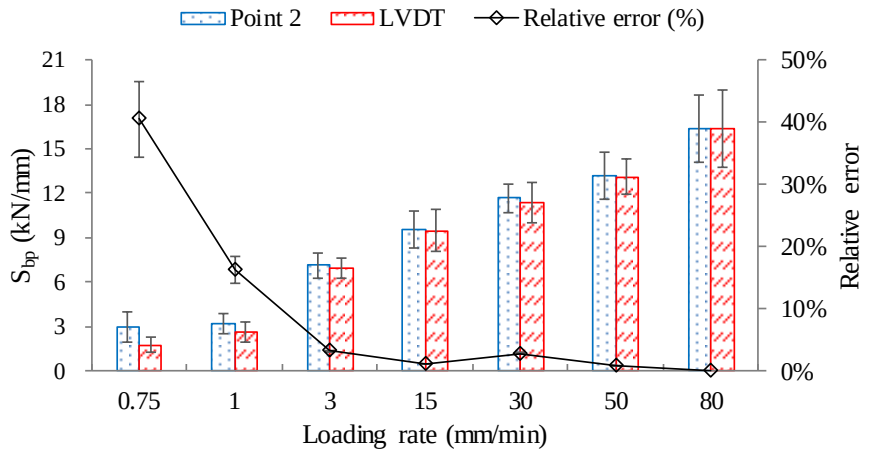

(a)

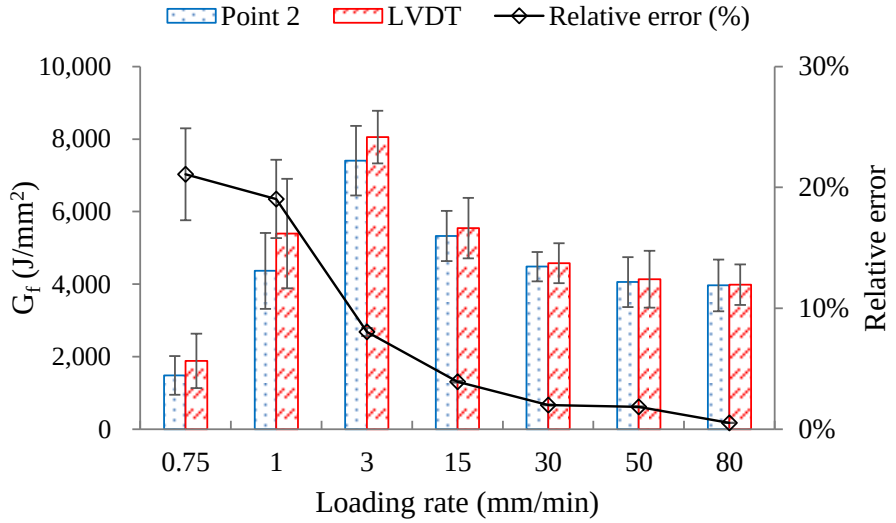

(b)

Figure 6 Cracking indexes and relative errors calculated by load-displacement curve from LVDT and Point 2 at different loading rates: (a) S_{bp}; (b) G_f.

5.2 Influence of the materials' factors

5.2.1 Effect of the binder film thickness and filler content on stiffness and fracture energy

According to the experimental matrix design, three levels of binder film thickness and four levels of filler content were prepared for the testing. Figure 7 shows the calculated low-temperature performance indicators including S_{bp} and G_f. As Figure 7(a) demonstrates, if the binder film thickness or the filler content is higher, S_{bp} of the

mortar under ST aging condition is lower. When it comes to the LT aging condition, as can be seen in Figure 7(b), asphalt mortars with higher binder film thickness still exhibit lower S_{bp} at each filler content. However, the S_{bp} of mortars with a filler content of 10.5% and 11% become close to each other. As illustrated in Figure 7(c) and (d), the fracture energy (G_f) is higher in value if the binder film thickness is thicker when the filler content is fixed. Additionally, it is worth noting that when the filler content increases from 10.5% to 11%, the G_f of mortar at ST aging condition has no increment, but even exhibits a slight decreasing trend, which indicates that there is an optimal filler content to reach the highest fracture energy for the asphalt mortar.

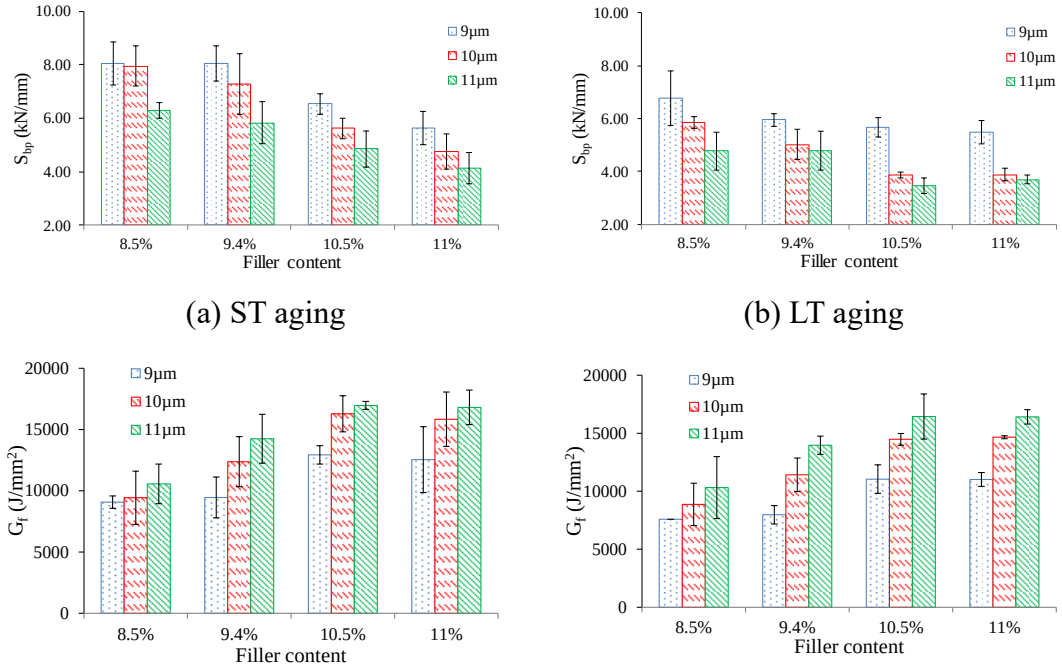

(a) ST aging (b) LT aging

(c) ST aging (d) LT aging

Figure 7 S_{bp} of asphalt mortar under short-term (a) and long-term (b) aging conditions and G_f under both short-term (c) and long-term (d) aging conditions.

5.2.2 Effect of the binder film thickness and filler contents on the aging rate

Figure 8 shows one typical changing pattern of the load-displacement curves caused by ST aging and LT aging. It was found that the peak load and the area under the load-displacement curve decrease significantly after LT aging. Also, it was noticed that the S_{bp} of the mortar sample decreases from ST aging to LT aging, which indicates that LT aging may change the stiffness of asphalt mortar at low temperature.

Normally, the oxidation aging leads to increment of the stiffness of asphalt binder and make it more brittle and harder caused by the loss of oily components by volatility or absorption. But, when it comes to LT oxidation aging, the mechanism of the aging effect becomes more complicated considering the changes in composition or molecular structure and the interface between binder and aggregate.

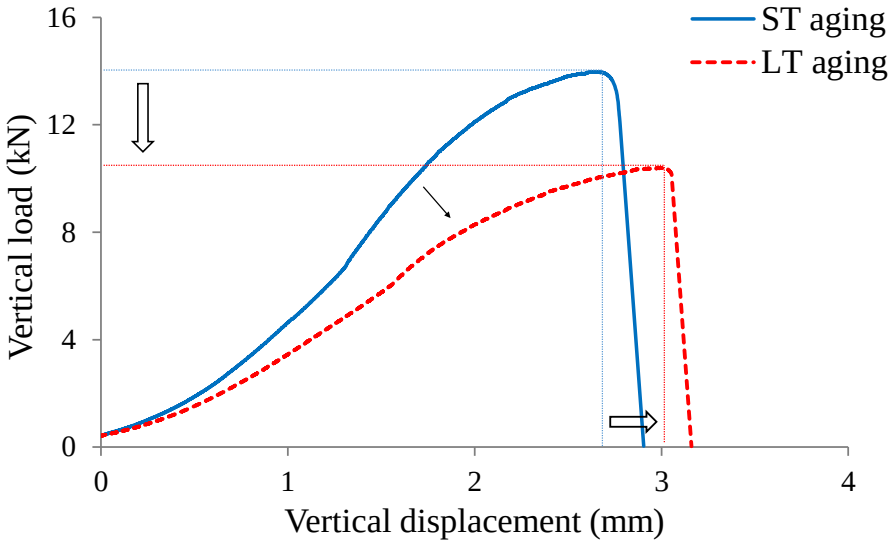

Figure 8 Load-displacement curves of F 9.4-T 10 mortar after ST and LT aging.

In this paper, to simplify the expression of the aging effect, the changing rate of fracture energy (G_f) after LT aging was considered to quantify the aging rate as defined in Equation 5. It does not necessarily mean that the material exhibits a better crack resistance or not if you have a higher aging rate. Higher aging rate indicates the long-term aging changed the fracture energy of the sample more.

$$Aging\ \ rate = \frac{G_f(ST) - G_f(LT)}{G_f(ST)} \tag{5}$$

where G_f (ST) = the fracture energy of asphalt mortar at low temperature after 4h loose mix aging, J/mm^2; and G_f (LT) = the fracture energy of asphalt mortar at low temperature after 4h loose mix aging, J/mm^2.

As illustrated in Figure 9, the aging rate of different mortar samples with the same filler content decrease significantly with the increasing of binder film thickness,

which means that the LT oxidation aging impacts the fracture energy more when the binder film thickness is thinner. The influence of filler contents on the aging rate is not remarkable compared to the influence of binder film thickness.

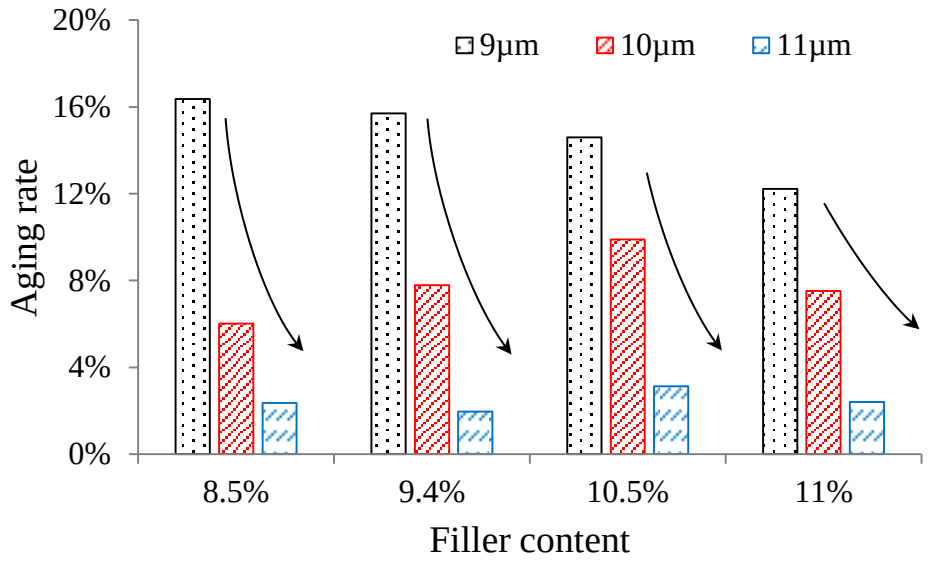

Figure 9 Aging rate of different asphalt mortars with different filler contents and binder film thicknesses.

To further evaluate whether the effects of filler content and film thickness on aging rate are statistically significant, a two-way Analysis of Variance (ANOVA)) with a 95% confidence was performed. The ANOVA results are presented in Table 2. The p-value of the factor of binder film thickness is less than 0.05, which indicates that binder film thickness significantly affects the aging rate. However, it is not clear how the filler content impact the low temperature performance of asphalt mortar based on currently collected data.

Table 2 Summary of ANOVA results.

Source	Factor	Degree of freedom	Sum of squares	F value	P-value
Aging rate	Filler content	3	0.000066	0.20	0.89587
	Binder film thickness	2	0.013763	40.74	**0.00032**

6. Findings and Conclusions

In this study, the SCB test was proposed to evaluate the low-temperature performance of asphalt mixture at the mortar scale. The DIC method was used to analyze the creep deformation in the SCB test, and furtherly verify the validation of the testing results. The effects of various factors, including binder film thickness, filler content, and aging condition (short-term aging and long-term aging), on the cracking indexes were investigated. The following major findings and conclusions were obtained:

1) Based on the basic shape of the load-displacement curve from the SCB mortar test, two cracking indexes, before-peak slope (S_{bp}) and fracture energy (G_f), were found to be suitable for evaluating the low-temperature cracking performance of asphalt mortar. Higher S_{bp} indicates stiffer asphalt mortar, and higher G_f indicates better cracking resistance of asphalt mortar.
2) According to the results of DIC analysis, most of the local creep deformations at all loading rates are within a 1cm area close the top of the SCB sample. More obvious local creep deformation can be found when the loading rate is lower and even crushing can be observed when the loading rate is 0.075mm/min.
3) With the increase of the loading rate, the relative errors of both cracking indexes (S_{bp} and G_f) from the load-displacement curves with or without the creep deformation decrease sharply. The loading rate of 3mm/min is acceptable at the temperature of -10ºC for the SCB mortar test. Since the relative errors in both the S_{bp} and G_f caused by the local deformation are less than 10%, and the variations of the relative errors caused by the local compressive creep are less than 5%, the

error caused by the local deformation is considered predictable and controllable.

4) According to the results of SCB mortar test in this study, higher binder film thickness and filler content in general result in lower S_{bp} and higher G_f of asphalt mortar. Besides, the statistical analysis shows that the aging rate of asphalt mortar is affected significantly by the binder film thickness, but the effect of the filler content is not statistically significant.

Acknowledgment

The authors thank the financial support from the National Natural Science Foundation of China (No. 51708201), Natural Science Foundation of Hunan Province (No. 2019JJ50064) and Fundamental Research Funds for the Central Universities (No. 531118010050).

Reference

[1] Jiang, J., Ni, F., Gu, X., Yao, L., & Dong, Q. (2019). Evaluation of aggregate packing based on thickness distribution of asphalt binder, mastic and mortar within asphalt mixtures using multiscale methods. *Construction and Building Materials*, 222, 717-730.

[2] Li, Q., Chen, X., Li, G., & Zhang, S. (2018). Fatigue resistance investigation of warm-mix recycled asphalt binder, mastic, and fine aggregate matrix. *Fatigue & Fracture of Engineering Materials & Structures*, 41(2), 400-411.

[3] Zaumanis, M., Poulikakos, L. D., & Partl, M. N. (2018). Performance-based design of asphalt mixtures and review of key parameters. *Materials & Design*, 141, 185-201.

[4] Zhou, Z., Gu, X., Dong, Q., Ni, F., & Jiang, Y. (2019). Low-and intermediate-temperature behaviour of polymer-modified asphalt binders, mastics, fine aggregate matrices, and mixtures with Reclaimed Asphalt Pavement material. *Road Materials and Pavement Design*, 1-30.

[5] Huang, W., & Lv, Q. (2017). Investigation of Critical Factors Determining the Accuracy of Binder Bond Strength Test to Evaluate Adhesion Properties of

Asphalt Binders. *Journal of Testing and Evaluation*, 45(4), 1270-1279.

[6] Khattak, M. J., Baladi, G. Y., & Drzal, L. T. (2007). Low temperature binder-aggregate adhesion and mechanistic characteristics of polymer modified asphalt mixtures. *Journal of materials in civil engineering*, 19(5), 411-422.

[7] Zhao, Y., Ni, F., Zhou, L., & Jiang, J. (2017). Heterogeneous fracture simulation of asphalt mixture under SCB test with cohesive crack model. *Road Materials and Pavement Design*, 18(6), 1411-1422.

[8] Li, Q., Li, G., Ma, X., & Zhang, S. (2018). Linear viscoelastic properties of warm-mix recycled asphalt binder, mastic, and fine aggregate matrix under different aging levels. *Construction and Building Materials*, 192, 99-109.

[9] Yan, J., Leng, Z., Li, F., Zhu, H., & Bao, S. (2017). Early-age strength and long-term performance of asphalt emulsion cold recycled mixes with various cement contents. *Construction and Building Materials*, 137, 153-159.

[10] Suresha, S. N., & Ningappa, A. (2018). Recent trends and laboratory performance studies on FAM mixtures: A state-of-the-art review. *Construction and Building Materials*, 174, 496-506.

[11] Ding, X., Ma, T., Gu, L., & Zhang, Y. (2020). Investigation of surface micro-crack growth behavior of asphalt mortar based on the designed innovative mesoscopic test. *Materials & Design*, 185, 108238.

[12] Zhu, Y., Dave, E. V., Rahbar-Rastegar, R., Daniel, J. S., & Zofka, A. (2017). Comprehensive evaluation of low-temperature fracture indices for asphalt mixtures. *Road Materials and Pavement Design*, 18(sup4), 467-490.

[13] Jiang, J., Ni, F., Dong, Q., Zhao, Y., & Xu, K. (2018). Fatigue damage model of stone matrix asphalt with polymer modified binder based on tensile strain evolution and residual strength degradation using digital image correlation methods. *Measurement*, 123, 30-38.

[14] Sadeq, M., Al-Khalid, H., Masad, E., & Sirin, O. (2016). Comparative evaluation of fatigue resistance of warm fine aggregate asphalt mixtures. *Construction and Building Materials*, 109, 8-16.

[15] Riccardi, C., Falchetto, A. C., Wistuba, M. P., & Losa, M. (2017). Fatigue

comparisons of mortars at different volume concentration of aggregate particles. *International Journal of Fatigue*, 104, 416-421.

[16] Underwood, B. S., & Kim, Y. R. (2013). Effect of volumetric factors on the mechanical behavior of asphalt fine aggregate matrix and the relationship to asphalt mixture properties. *Construction and Building Materials*, 49, 672-681.

[17] Nabizadeh, H., Haghshenas, H. F., Kim, Y. R., & Aragão, F. T. S. (2017). Effects of rejuvenators on high-RAP mixtures based on laboratory tests of asphalt concrete (AC) mixtures and fine aggregate matrix (FAM) mixtures. *Construction and Building Materials*, 152, 65-73.

[18] Zhu, J., Alavi, M. Z., Harvey, J., Sun, L., & He, Y. (2017). Evaluating fatigue performance of fine aggregate matrix of asphalt mix containing recycled asphalt shingles. *Construction and Building Materials*, 139, 203-211.

[19] Karki, P., Li, R., & Bhasin, A. (2015). Quantifying overall damage and healing behaviour of asphalt materials using continuum damage approach. *International Journal of Pavement Engineering*, 16(4), 350-362.

[20] Gong, X., Romero, P., Dong, Z., & Li, Y. (2017). Investigation on the low temperature property of asphalt fine aggregate matrix and asphalt mixture including the environmental factors. *Construction and Building Materials*, 156, 56-62.

[21] Caro, S., Sánchez, D. B., & Caicedo, B. (2015). Methodology to characterise non-standard asphalt materials using DMA testing: application to natural asphalt mixtures. *International Journal of Pavement Engineering*, 16(1), 1-10.

[22] Ma, T., Mahmoud, E., & Bahia, H. U. (2010). Estimation of reclaimed asphalt pavement binder low-temperature properties without extraction: Development of testing procedure. *Transportation research record*, 2179(1), 58-65.

[23] Swiertz, D., Mahmoud, E., & Bahia, H. U. (2011). Estimating the effect of recycled asphalt pavements and asphalt shingles on fresh binder, low-temperature properties without extraction and recovery. *Transportation research record*, 2208(1), 48-55.

[24] Jiang, J., Ni, F., Dong, Q., Wu, F., & Dai, Y. (2018). Research on the fatigue

equation of asphalt mixtures based on actual stress ratio using semi-circular bending test. *Construction and Building Materials*, 158, 996-1002.

[25] Ayatollahi, M. R., & Aliha, M. R. M. (2007). Fracture toughness study for a brittle rock subjected to mixed mode I/II loading. International Journal of Rock Mechanics and Mining Sciences, 44(4), 617-624.

[26] Huang, B., Shu, X., & Zuo, G. (2013). Using notched semi circular bending fatigue test to characterize fracture resistance of asphalt mixtures. *Engineering Fracture Mechanics*, 109, 78-88.

[27] Jiang, J., Dong, Q., Ni, F., & Zhao, Y. (2018). Effects of Loading Rate and Temperature on Cracking Resistance Characteristics of Asphalt Mixtures Using Nonnotched Semicircular Bending Tests. *Journal of Testing and Evaluation*, 47(4), 2649-2663.

[28] Yang, S., & Braham, A. F. (2017). Influence of binder grade, gradation, temperature and loading rate on R-curve of asphalt concrete. *Construction and Building Materials*, 154, 780-790.

[29] Im, S., Kim, Y. R., & Ban, H. (2013). Rate-and temperature-dependent fracture characteristics of asphaltic paving mixtures. *Journal of Testing and Evaluation*, 41(2), 257-268.

[30] Li, X., Braham, A. F., Marasteanu, M. O., Buttlar, W. G., & Williams, R. C. (2008). Effect of factors affecting fracture energy of asphalt concrete at low temperature. *Road materials and pavement design*, 9(sup1), 397-416.

[31] Kliewer, J. E., Zeng, H., & Vinson, T. S. (1996). Aging and low-temperature cracking of asphalt concrete mixture. *Journal of Cold Regions Engineering*, 10(3), 134-148.

[32] Falchetto, A. C., Moon, K. H., Wang, D., Riccardi, C., & Wistuba, M. P. (2018). Comparison of low-temperature fracture and strength properties of asphalt mixture obtained from IDT and SCB under different testing configurations. *Road Materials and Pavement Design*, 19(3), 591-604.

[33] Zegeye, E., Le, J. L., Turos, M., & Marasteanu, M. (2012). Investigation of size effect in asphalt mixture fracture testing at low temperature. *Road Materials and*

Pavement Design, 13(sup1), 88-101.

[34] Shao, X., Dai, X., & He, X. (2015). Noise robustness and parallel computation of the inverse compositional Gauss–Newton algorithm in digital image correlation. *Optics and Lasers in Engineering*, 71, 9-19.

[35] Shao, X., & He, X. (2017). Statistical Error Analysis of the Inverse Compositional Gauss-Newton Algorithm in Digital Image Correlation. In *International Digital Imaging Correlation Society* (pp. 75-76). Springer, Cham.

[36] Braham, A. F., & Mudford, C. J. (2012). Comparing the Slope of Load/Displacement Fracture Curves of Asphalt Concrete. In *7th RILEM International Conference on Cracking in Pavements* (pp. 997-1006). Springer, Dordrecht.

[37] Cerni, G., Cardone, F., & Colagrande, S. (2011). Low-temperature tensile behaviour of asphalt binders: Application of loading time–temperature–conditioning time superposition principle. *Construction and Building Materials*, 25(4), 2133-2145.